Journal of Thermal Science Vol.28, No.6 (2019) 1115−1128

https://doi.org/10.1007/s11630-018-1047-7 **Article ID: 1003-2169(2019)06-1115-14**

Optimizing Building Envelope Dimensions for Passive Solar Houses in the Qinghai-Tibetan Region: Window to Wall Ratio and Depth of Sunspace

LIU Zhijian[1,*], WU Di[1], LI Junyang[1], YU Hancheng[2], HE Baojie[3]

1. Department of Power Engineering, North China Electric Power University, Baoding, Hebei 071003, China
2. Department of Building Energy Conservation, Qinghai College of Architectural Technology, Xining 810002, China
3. Faculty of Built Environment, University of New South Wales, NSW 2052, Australia

Abstract: It has been a focus to reduce the energy consumption and improve the space heating performance of high-altitude buildings in winter seasons. In view of the abundant solar energy resources of the high-altitude region, the establishment of passive solar houses should be an effective strategy to deal with the problem of thermal comfort. Both window to wall ratio (WWR) and sunspace depth are of vital importance to determine the thermal comfort level of passive solar houses, while there are limited studies on analyzing their impacts on passive solar houses in high-altitude regions. Therefore, this study is designed to examine how WWR and sunspace depth affect space heating of passive solar houses in the Qinghai-Tibetan region. To be specific, the hourly radiation temperature variations and percentages of dissatisfaction of the residential building with different sunspace depth/WWR (including 0.9m/33%, 0.9m/45%, 0.9m/60%, 1.2m/33% and 1.5m/33%) were quantitatively examined. Results indicated that under the condition of 0.9m/45%, the overall average radiation temperature of the building was approximately 16°C during the entire heating season, which could better satisfy the heating requirements. Meanwhile, the average temperature was higher, and the thermal comfort level was better under the ratio of 45% or the depth of 1.5 m, when only an individual factor in either ratio or depth was considered. These findings can provide references for the determination of dimensions of passive solar houses in high-altitude regions.

Keywords: passive solar house, indoor thermal comfort, sunspace depth, *WWR* (window to wall ratio), *PPD* (Predicted Percent Dissatisfied)

1. Introduction

The current world is witnessing a rapid improvement in people's living quality, while a series of problems like energy shortcomings, greenhouse gas emissions and urban heat island effects emerge [1–3]. Renewable energy utilization has been extensively recognized as a sustainable approach to solve these issues. Moreover, the renewable energy utilization could be an outstanding alternative for space heating in plateau areas. In these areas, the oxygen content is so low that the conventional fuel combustion is difficult to burn completely, resulting in the

Received: June 3, 2018 Corresponding author: LIU Zhijian E-mail: zhijianliu@ncepu.edu.cn

Abbreviations

ε_0	blackness of the imaginary isothermic enclosed surface	*SC*	integrated shading coefficient
ε_j	blackness of *j*th surface	*SHGC*	solar heat gain coefficient
C_{mci}	solar radiation correction coefficient of door and window	*TL*	thermal load/W·m^{-2}
F_j	angle factor of *j*th surface	T_j	temperature of *j*th surface/K
M	metabolic heat production/W·m^{-2}	T_{mrt}	mean radiation temperature/K
PMV	predicted mean vote	*WWR*	window to wall ratio/%
PPD	predicted percent dissatisfied/%		

waste of fossil fuels, as well as severe threats to the human health and environment due to the harmful gases produced (such as NO, SO_2, CO) [4–8]. Fortunately, plateau areas are generally characterized by rich solar energy resource, offering great potentials to solve these issues [9].

The passive solar house is a common means of solar energy utilization in practice [10–14]. Many researchers have carried out studies on temperature levels in passive solar houses to examine the feasibility of them in cold and plateau areas [15–17]. For example, in Northern Italy, Salvalai et al. [18] practically built an integrated system which was applied in several houses. The system included heat recovery equipment, solar photovoltaic panels, radiant floor heating system and electric boiler. Based on experimental tests, they revealed that the available heat in the studied houses could reach 30 kWh/(m^2·a). Liu et al. [19] experimentally examined indoor temperatures in passive solar houses of Qinghai-Tibetan plateau and found that Qinghai-Tibetan plateau was suitable for the construction of the passive solar house. Meanwhile, main approaches that can improve performances of the solar heating system and its optimization for building envelope have been studied. Rekstad et al. [20] comparatively investigated the space heating of two passive houses that were respectively equipped with solar heating system and the air-water heat pump system, in the situation of cold climate region. Due to the less auxiliary energy demand, the solar heating system had better energy saving performance than air-water heat pump system in the monitoring period. In order to further explore effective methods to improve indoor temperature level, an integrated space heating system was built by Shan et. al., which included a solar collector, air source heat pump and passive sunspace [21]. The running scheme was proposed by debugging which could satisfy the indoor heating requirement and had high energy efficiency. Additionally, the application of Trombe wall that characterized with good heating collection and heat storage properties was recommended in the passive solar house, in which reasonable opening and closing of the ventilation holes could improve its average heat efficiency [22–24]. However, the utilization of passive solar house is, to a large extent, constrained by the investment-payback period, since it is excessively long when considering the initial investment for auxiliary equipment and expensive operational/maintenance costs of the heating system [25]. Therefore, it is essential to think about how to reduce the cost of passive solar house reconstruction, which is particularly significant in some low economic regions.

It shows that the sunspace and direct gain windows plays an importance role in determining the space heating of passive solar houses [5,26,27]. Lu et al. [28] and Zhang et al. [29] suggested that buildings with additional sunspace had significant effects on energy saving in cool regions. Chiesa et al. [30] pointed out that sunspace technology could be widely utilized to reduce the energy consumption. On the basis of climatic condition and building configuration in central and southern Europe, they presented the suitable technology, with respect to sunspace, to design or retrofit the building envelope for lowering energy consumption. Bataineh et al. [31] also verified that sunspace could be an advisable approach to the reduction of heating load in winter. In the context of Amman, Jordan, six configurations of sunspace with different ratio of glazed surface area to opaque surface area were compared, and the optimal structure with the inclined front surface was proposed. Schoenau et al. [32] examined the indoor thermal environment of sunspace under various operating modes, e.g. the use of blinds and exhaust fans in Northern American. Li et al. [33] found that window to wall ratio (*WWR*) could influence the indoor temperature, where the average indoor temperature could improve about 5°C with the *WWR* increasing from 40% to 70% for the southern room. Nevertheless, the reasonable design dimensions of sunspace and *WWR* have no specific data analysis and references in plateau areas.

Therefore, in order to reduce the energy consumption for space heating on one hand, and improve the indoor

thermal environment on the other hand, this study is to investigate the impacts of *WWR* dimension and sunspace depth of passive solar houses in Qinghai-Tibet region. To be specific, a residential building has been built as the demonstration project on Qinghai-Tibetan plateau, to obtain the reasonable dimensions of sunspace and direct gain windows, in which effects of sunspace depth and *WWR* on the indoor thermal environment are explored. Furthermore, under different conditions of sunspace depth / *WWR* (0.9m/33%, 0.9m/45%, 0.9m/60%, 1.2m/33% and 1.5m/33%), the hourly radiation temperature variations and predicted percent dissatisfied (*PPD*) of different rooms are numerically examined in heating season by using IES (VE) software. The findings of this study are valuable to offer references for the design and application of solar house in high altitude regions.

2. Study Object

The investigation was carried out based on residential buildings in the Wangtun village of Qinghai Tibetan plateau, China (latitude 35°97′N, longitude 101°47′E, altitude 2367 m). The Wangtun village is characterized with severe cold climate, with the maximum and minimum mean monthly temperature of 23°C (August) and -5°C (January), respectively. Its annual solar energy potential ranges between 1440 kWh/m^2 and 1750 kWh/m^2 [34]. For the single-storey residence studied, it is very typical on the plateau in aspects of building structure, room layouts and southern-orientation [35]. The residence covers a floor area of 84 plane m^2, with the plane dimensions of 12320 mm (length in east-west direction) and 6920 mm (width in north-south direction), as well as 3500 mm in height. More detailed information is given in Table 1 and Table 2. To be specific, this building consists of a living room, two bedrooms, a sunspace, a kitchen, a toilet and a storage room, whose detailed configurations are exhibited in Figure 1. For the sunspace, it is embedded in the building, with its southern envelope composed by glass. For remaining external walls of this building, they are embedded with a thermal insulation layer. In addition, the Chinese *kang* in room 5 is adopted as the internal heat source of this building. During the monitoring period, the *kang* was in operation and its heat power reached 800 W.

To investigate impacts of depths and *WWRs* on building space heating, we established various typical buildings with different depths and *WWRs*. According to design specifications and many pilot projects, the sunspaces should have depths of 0.9 m, 1.2 m and 1.5 m and *WWRs* of 33%, 45% and 60% [34]. Accordingly, we built five typical models. As shown in Figure 2(a), the depth and *WWR* of the model are 0.9 m and 33%, respectively. Likewise, two other models with parameters of 0.9m/45% and 0.9m/60% are shown in Figure 2(b) and Figure 2(c). Based on this, temperature variations along *WWRs* can be simulated and studied. In addition, two extra models with 1.2m/33% and 1.5m/33% were built, as shown in Figure 2(d) and Figure 2(e) respectively, to further investigate how depths influence indoor temperature, in combination of the model of 0.9m/33%. Furthermore, the elevation dimension of the sunspace is 4660 mm × 3200 mm, and dimensions of window and door on the public wall which separates the sunspace from the bedroom are 2100 mm × 1700 mm and 2100mm× 910 mm, respectively, as indicated in Figure 1 and Figure 2 (a).

In each scenario, two clerestory windows with sizes of 1500 mm × 800 mm were preserved on the southern wall of storage rooms to receive more solar radiation

Table 1 Characteristics of study building

Total floor area of building /m^2	Volume of building /m^3	Total area of envelope (including windows and roof) /m^2	Bulk coefficient of building	*SC*	*SHGC*	C_{mci}
84.15	283.73	212.04	0.75	0.68	0.78	0.41

Table 2 Areas of windows and walls of building envelope

Items	*WWRs* /%	Areas of envelope (including windows) /m^2	Areas of external windows /m^2
Southern direction	33	42.70	14.10
	45		19.22
	60		25.62
Northern direction	0	39.37	0
Eastern direction	11	22.91	2.52
Western direction	4	22.91	0.92
Roof	0	84.15	0

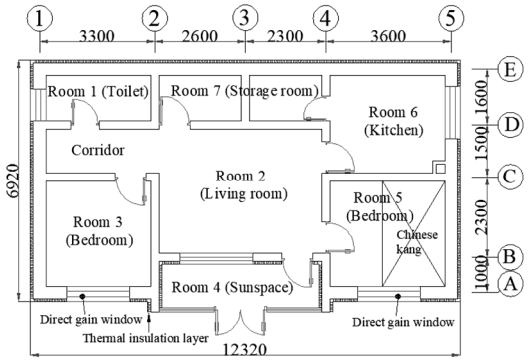

Fig. 1 Layout plan of the residential building (Unit: mm)

(Fig. 2(a)). Technically, the clerestory windows act as solar-enhanced buffers along the northern edge of the living room. The material utilized in the sunspace is aluminum- plastic composite energy-saving material (70 series), having promising capacities to reduce heat loss. The external window is a kind of swinging casement window with triplex glass, while the external wall adopts B1- graphite insulating board, whose heat conductivity coefficient is 0.032 W/(m·K), to improve building insulation. The specific materials used in each building component and corresponding heat transfer coefficient are given in Table 3.

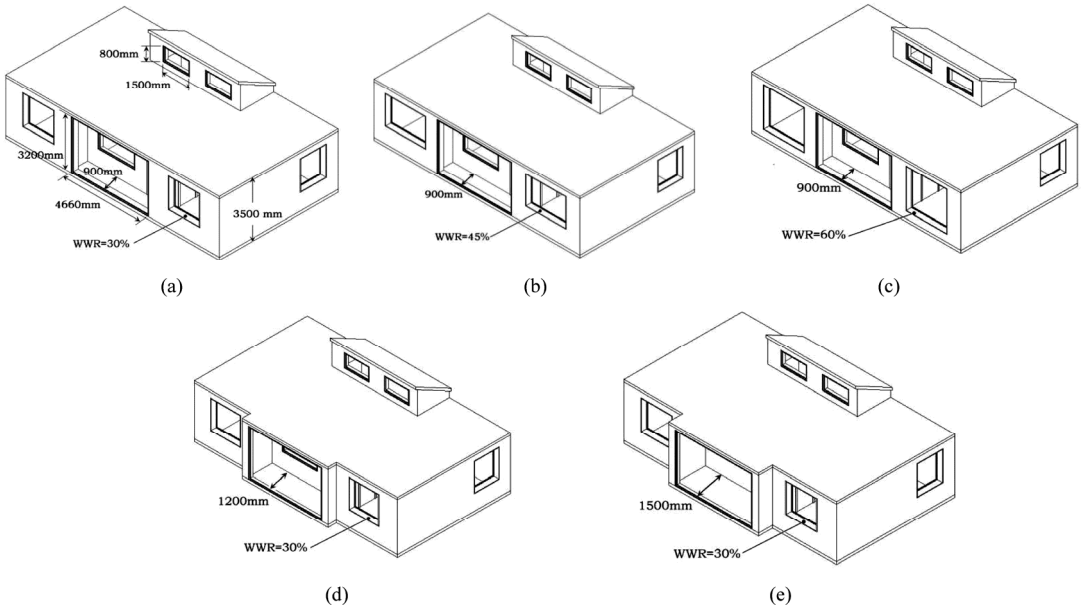

Fig. 2 Simulation model of the residential building with different conditions. (a) model with 0.9m/33%; (b) model with 0.9m/45%; (c) model with 0.9m/60%; (d) model with 1.2m/33%; (e) model with 1.5m/33%.

Table 3 Total heat transfer coefficient and materials of the building envelope

Items		Materials	Heat transfer coefficient /W·m^{-2}·K^{-1}
External wall		B1-graphite insulating board (100 mm), colliery wastes brick (370 mm)	0.29
Opaque section of roof		B1-graphite insulating board (200 mm), cement cinder (30mm), reinforced concrete (120 mm)	0.15
External window		Swinging casement windows with triplex glass (4+9+4+9+4)	2.20
Ground		B1-graphite insulating board (150 mm)	0.15
External door		Aluminum-plastic composite energy saving material (70 series)	1.70
Sunspace	Transparent section	Aluminum-plastic composite energy saving material (70 series)	1.80
	Opaque section	B1-graphite insulating board (100 mm), colliery wastes brick (370 mm)	0.29

3. Theoretical Analyses and Methodologies

3.1 Simulation software and parameters setting

In this study, IES (VE) was used to simulate indoor environment and further obtain the hourly mean indoor radiation temperatures and predicted percent dissatisfied (*PPD*), since IES (VE) simulation was a robust and reliable approach to mimic hourly thermal performances under various situations with considerations of geographical and climatic locations [36]. This has been evidenced to be a wide range of studies on indoor thermal

comfort [37–40].

The meteorological parameters of Xining city were directly loaded into IES (VE) for further simulation. The annual average radiation intensity of Xining is 1578kWh/m^2, while its annual average temperature is 6.3°C, with the maximum and minimum monthly temperature of 17.8°C and -7.3°C, respectively. Comparatively, the occupancy, building infiltration rates and outdoor wind fluctuation were set as default. The absorptivity of human clothing and the attitude correction coefficient were set as 0.97 and 0.72, respectively. Furthermore, the 3D geometric model was established via importing the DXF format files, as the building process presented in Figure 3. According to previous research, the reasonable southern window opening and closing behaviors should be basically consistent with the sunrise and sunset time [41]. Thus, the direct gain windows as well as all internal doors were completely open from 8:00 to 18:00, which was favorable for accepting solar radiation during the day and avoiding heat losses in the night. Because we only stood on analyzing impacts of ambient temperature on indoor thermal comfort for the optimization of *WWRs* and depths, the IES (VE) simulation had not set up mechanical ventilation equipment to accelerate the convective heat transfer process and the outdoor air flow was ignored.

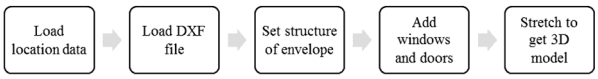

Fig. 3 Flow chart for building model

3.2 Mean radiation temperature

When the exchanged radiation heat between the human body and the imaginary isothermic enclosed surface is equivalent to that between the human body and the actual non-isothermal enclosed surface, the temperature of the imaginary isothermic enclosed surface is then defined as the mean radiation temperature T_{mrt}, [K]. T_{mrt} is expressed by *Eq.*(1):

$$T_{\mathrm{mrt}} = \left(\frac{1}{\varepsilon_0} \sum_{j=1}^{k} \left(F_j \varepsilon_j T_j^4 \right) \right)^{1/4} \tag{1}$$

where F_j represents the angle factor of the jth surface. T_j is the temperature of the jth surface, [K]. ε_j is the blackness of jth surface. ε_0 is the blackness of the imaginary isothermic enclosed surface. Radiation temperature that can evaluate the temperature the body feels could more exactly reflect the thermal comfort level.

3.3 Predicted percentages of dissatisfaction

Predicted percent dissatisfied (*PPD*) refers to the comprehensive evaluation of the physical and psychological dissatisfied degree of the objective environment that people feel, [%]. In this study, *PPD* was adopted as an indicator to assess the thermal comfort level in real time. The equation of *PPD* can be expressed by *Eq.* (2) [42-45]. Predicted mean vote (*PMV*) is also an indicator utilized to reflect the comfort level, which can be expressed by *Eq.* (3):

$$PPD = 100 - 95 \times \exp\left[-\left(0.03353 \times PMV^4 + 0.2179 \times PMV^2 \right) \right] \tag{2}$$

$$PMV = \left[0.303 \times \exp\left(-0.036 \times M \right) + 0.0275 \right] \times TL \tag{3}$$

where, M is the metabolic heat production, [W/m^2]. *TL* (Thermal Load) represents the difference between the amount of heat produced by the body and that lost from the body to the outside, [W/m^2].

4. Results and Analysis

The variations of hourly indoor radiation temperature and *PPD* in heating season (from October 15 to April 15 the next year) are analyzed in this section, where hourly radiation temperatures in various scenarios are compared in Figure 4, Figure 5, Figure 6 and Figure 7, while *PPD* variations in different rooms are presented in Table 4. The box-plot diagram displays the values of a series of indicators including mean, median, maximum, minimum, 1% percentile, 99% percentile, 25% percentile, 75% percentile, 10% percentile and 90% percentile hourly radiation temperatures.

4.1 Temperature variations of different rooms in various conditions

Temperature variations of different rooms with sunspace depths and *WWRs* during heating season are presented in Figure 4. In the scenario of 0.9m/33%, the highest and lowest temperatures of Room 4 (the sunspace) were approximately 50°C and -5°C, respectively, while its daily temperature fluctuated significantly, as indicated in Figure 4 (a). It reveals that the sunspace temperature is sensitive to outdoor temperature variations. Indoor radiation temperature of other rooms underwent consistent trends but witnessed small differences. Moreover, the indoor temperatures of all rooms varied significantly with the seasons. For instance, the lower temperature occurred mainly in cold months (including December, January and February). The average radiation temperatures of Room 1-Room 7 were respectively 3.82°C, 5.42°C, 6.07°C, 10.32°C, 5.49°C, 3.90°C and 4.98°C (Figure 4 (b)). Due to the smaller *WWR*, solar heats received by buildings through the direct gain windows were quite limited, resulting in lower average radiation temperatures ranging between 3°C and 11°C.

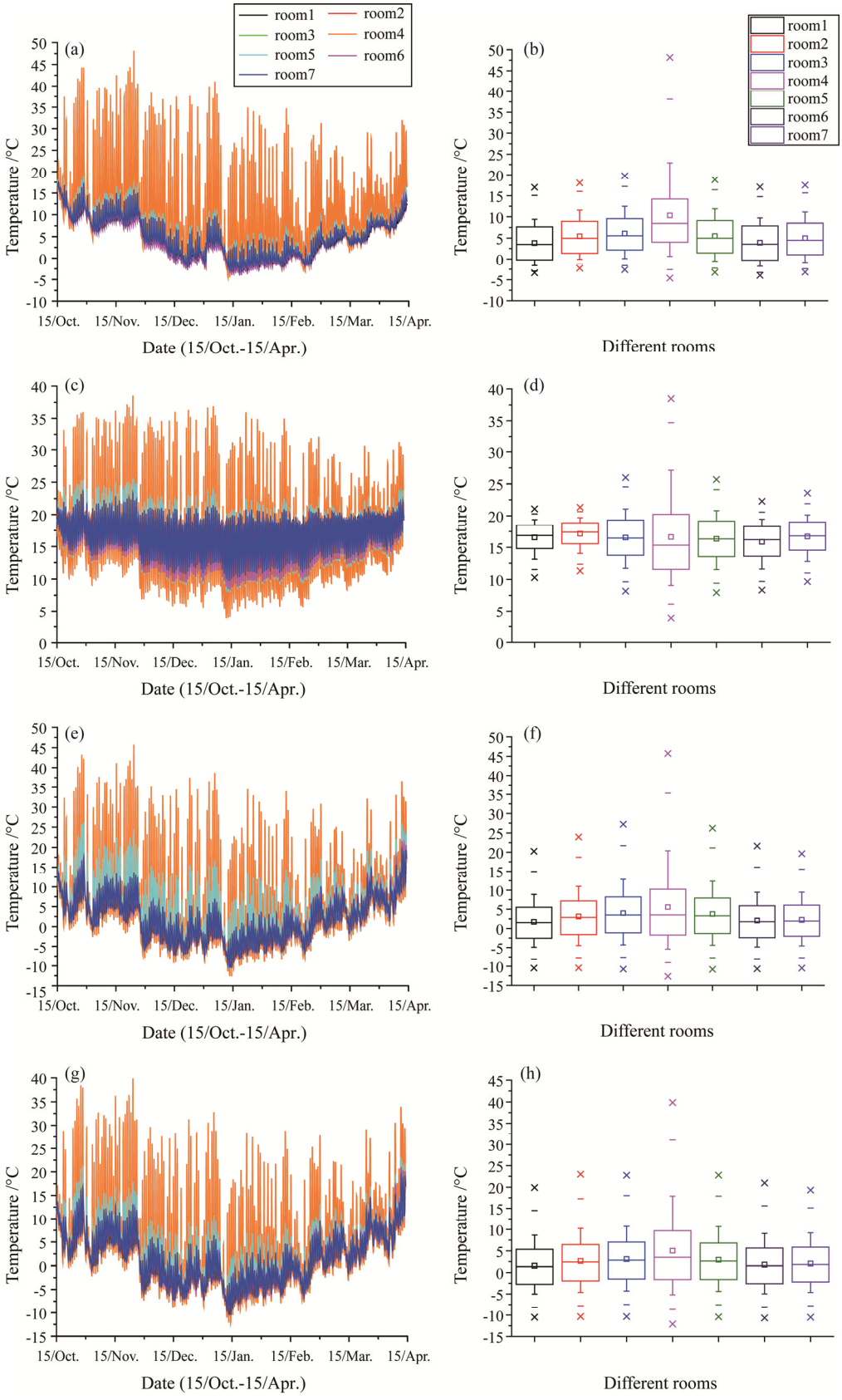
(a)
room1
room2
room3
room4
room5
room6
room7
Temperature /°C
Date (15/Oct.-15/Apr.)
15/Oct. 15/Nov. 15/Dec. 15/Jan. 15/Feb. 15/Mar. 15/Apr.
(b)
Different rooms
(c)
(d)
(e)
(f)
(g)
(h)

Continuation Fig.4

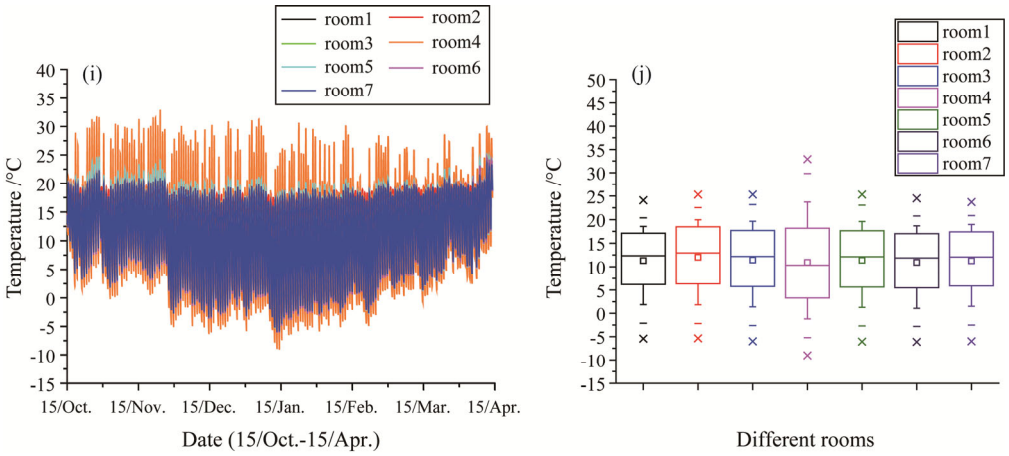

Fig. 4 The variations of hourly temperatures with different rooms during heating season. (a) hourly temperature variation under 0.9m/33% condition; (b) hourly temperature histogram under 0.9m/33% condition; (c) hourly temperature variation under 0.9m/45% condition; (d) hourly temperature histogram under 0.9m/45% condition; (e) hourly temperature variation under 0.9m/60% condition; (f) hourly temperature histogram under 0.9m/60% condition; (g) hourly temperature variation under 1.2m/33% condition; (h) hourly temperature histogram under 1.2m/33% condition; (i) hourly temperature variation under 1.5m/33% condition; (j) hourly temperature histogram under 1.5m/33% condition.

For the case of 0.9m/45%, insignificant differences existed among the radiation temperatures of all rooms during cold months, as presented in Fig. 4 (c). However, these temperatures were vulnerable to diurnal- nocturnal temperatures. The radiation temperatures of Room 4 varied sharply in one day and corresponding temperature discrepancy exceeded 35°C. For Room 3 and Room 5, their temperature fluctuated much more intensively than other rooms' temperature (except Room 4), because the larger direct gain windows led to more heat losses during the night. It is worth mentioning that almost all temperatures of seven rooms were consistently above 5°C and the average temperature of the building was around 16°C during the entire heating season, even in cold months. Moreover, the average radiation temperatures of all rooms were 16.55°C, 17.13°C, 16.52°C, 16.62°C, 16.33°C, 15.85°C and 16.68°C respectively, which could well satisfy the heating requirements (Fig.4(d)).

Considering the apparent temperature variations, the hourly temperatures of core zones (living room and two bedrooms) under the situation of 0.9m/45% were further investigated, during time period between January 1 and January 5 (in coldest month), as presented in Figure 5. It is observed that all hourly temperatures varied in a similar pattern, and the lowest temperatures of bedrooms and the living room were above 10°C and 13°C, respectively, achieving better space heating.

Each room (except room 4) followed a similar temperature trend in the scenario of 0.9m/60%, and this trend was obviously sensitive to cold months and diurnal-nocturnal temperatures. The maximum daily temperature difference reached 15°C, which was observed in Room 3

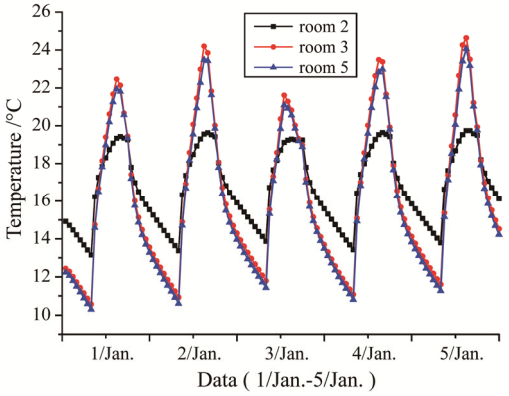

Fig. 5 The variations of hourly radiation temperatures between January 1 and January 5 in the scenario of 0.9m/45%

and Room 5 (Figure 4 (e)). Room 4 saw a large temperature fluctuation, with the highest temperature of 45°C and the lowest temperature of -13°C (Figure 4 (f)). Meanwhile, the average radiation temperature of each room was 1.75°C, 3.11°C, 3.99°C, 5.56°C, 3.75°C, 2.06°C and 2.24°C, respectively, while the lowest temperatures of all rooms were around -10°C. Overall, the temperature level of the scenario of 0.9m/60%was low, showing its worse heating performance. This can be explained by the less heat inputs through sunspace due to short depth during the day, while more heat losses because of the large direct gain windows at night.

The temperature variations of all rooms in the condition of 1.2m/33%were similar to that of 0.9m/60% (Figure 4 (g) and (h)). The mean radiation temperatures of

Room 1- Room 7 were 1.56°C, 2.63°C, 3.09°C, 5.04°C, 2.93°C, 1.81°C and 2.06°C, successively. The temperature level of each room was low, with the lowest temperature of -10°C, resulted from lower heat absorption and higher heat dissipation.

The temperature variations of buildings that were characterized with 1.5m/33% and 0.9m/45%were similar, which were also affected by the diurnal-nocturnal temperature and cold months (Fig. 4 (i) and (j)). The average radiation temperatures of seven rooms were 11.31°C, 12.01°C, 11.41°C, 10.91°C, 11.36°C, 10.92°C and 11.24°C (1.5m/33%) respectively, fluctuating around 11°C.

In the scenarios of 0.9m/33%, 0.9m/60% and 1.2m/33%, the mean *PPD* of all rooms (except Room 4) was above 90% and the standard deviations were primarily not higher than 20% (Table 4). Therefore, all rooms underperformed in thermal comfort level in these conditions. Concerning the scenario of 0.9m/45%, the mean *PPD* of Room 4 and other rooms were 44% and around 24%-35%, respectively. This shows that the building characterized with 0.9m/45% performed well in overall thermal comfort. More outstandingly, both *PPD* and its standard deviation of Room 2 were the lowest, indicating that Room 2 experienced the optimal thermal comfort amongst all rooms. In addition, the average *PPD* and standard deviation of each room under 1.5m/33% were higher than 50% and 40% respectively, which could not guarantee the indoor thermal comfort.

4.2 The influence of WWR on temperature

Performances of typical rooms (including Room 1, Room 2, Room 3 and Room 4) were selected to investigate the impacts of *WWR* on the indoor thermal environment during the heating season, and their radiation temperature variations are presented in Figure 6.

To start with, Rooms 1 and Room 2 shared similar trends in temperature variations (Fig. 6 (a)-(d)), primarily reflected by the stratified hourly radiation temperatures in accordance to different *WWRs*. Temperature level corresponding to the *WWR* of 45% was the highest, followed by 33% and the lowest 60%. The average radiation temperatures under these three conditions (33%, 45%, 60%) were about 5°C, 17°C and 3°C respectively. When the *WWR* was 45%, the temperature fluctuation was inferior during the entire heating season, even in cold months. Comparatively, however, the hourly radiation temperatures were obviously lower in December, January and February when the *WWR* was either 33% or 60%. This means indoor radiation temperatures were undesirable in cold months under these two situations. Additionally, the indoor radiation temperature in the scenario of 60% suffered large daily temperature fluctuation, which was in relation to the large area of windows, allowing environment temperature to disturb indoor temperature easily.

Room 3, the southern side room, was directly affected by the direct gain window. Its indoor radiation temperature varied greatly along day and night alternation, and its temperature fluctuated significantly in these three *WWR* scenarios during the heating season (Figure 6 (e) and (f)). The average radiation temperatures were respectively around 6°C, 16°C and 4°C, in accordance to the *WWRs* of 33%, 45% and 60%. The highest and lowest temperature, about 27°C and -12°C in value, occurred in the condition of 0.9m/60%. Moreover, the average radiation temperature of *WWR*=45% was significantly higher than that of *WWR*=33% and *WWR*=60%.

Indoor radiation temperature of Room 4 varied greatly between day and night (Figure 6 (g) and (h)). The average radiation temperatures in three *WWR* scenarios were respectively 10°C, 17°C and 6°C (in order of 33%, 45% and 60%). The highest temperature level appeared in the scenario of 45%. When the ratio was either 33% or 60%, the temperature of Room 4 underwent a large-scale fluctuation, with the highest temperature reaching 48°C or 45°C, respectively. However, the lowest temperature of Room 4 was -12°C appearing with WWR of 60%.

Table 4 *PPD* of different rooms during the heating season

	Items	Room1	Room2	Room3	Room4	Room5	Room6	Room7
0.9m/33%	Mean /%	96.36	93.25	0.79	77.67	92.28	95.92	93.82
	Standard deviation /%	9.89	13.75	17.80	31.01	15.91	10.43	13.56
0.9m/45%	Mean /%	27.83	24.49	33.02	44.00	33.94	34.41	28.96
	Standard deviation /%	22.4	19.86	28.29	33.43	28.98	28.33	24.14
0.9m/60%	Mean /%	97.01	93.75	90.59	85.42	91.38	96.27	96.36
	Standard deviation /%	10.22	16.82	21.65	28.05	20.59	11.95	11.39
1.2m/33%	Mean /%	97.28	95.04	94.18	85.85	94.47	96.72	96.65
	Standard deviation /%	9.69	14.42	15.86	27.62	15.39	11.10	10.81
1.5m/33%	Mean /%	53.94	52.09	54.19	58.2	54.28	55.21	54.46
	Standard deviation /%	40.68	41.55	41.36	41.67	41.39	41.16	41.04

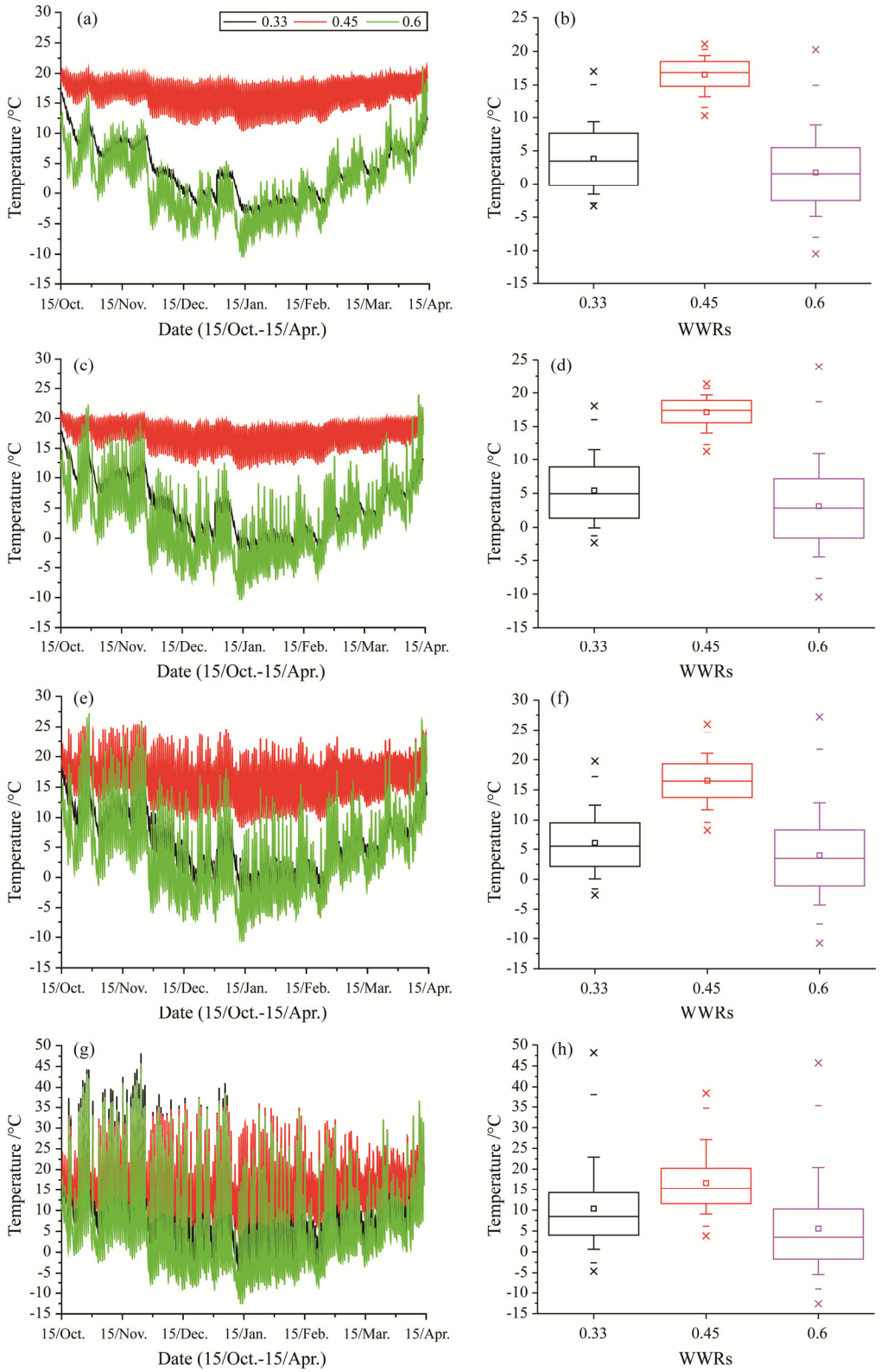

Fig. 6 The variations of hourly radiation temperatures with different *WWRs* during the heating season (Depth of sunspace is 0.9 m). (a) hourly temperature variation of room 1; (b) hourly temperature histogram of room 1; (c) hourly temperature variation of room 2; (d) hourly temperature histogram of room 2; (e) hourly temperature variation of room 3; (f) hourly temperature histogram of room 3; (g) hourly temperature variation of room 4; (h) hourly temperature histogram of room 4.

4.3 The impacts of sunspace depth on temperature

Temperature variations with sunspace depths of typical rooms, i.e. Room 1, Room 2, Room 3 and Room 4, are shown in Figure 7. The temperature variations of Room 1, Room 2 and Room 3 with different depths were similar (Figure 7 (a)-(f)). The thermal comfort level

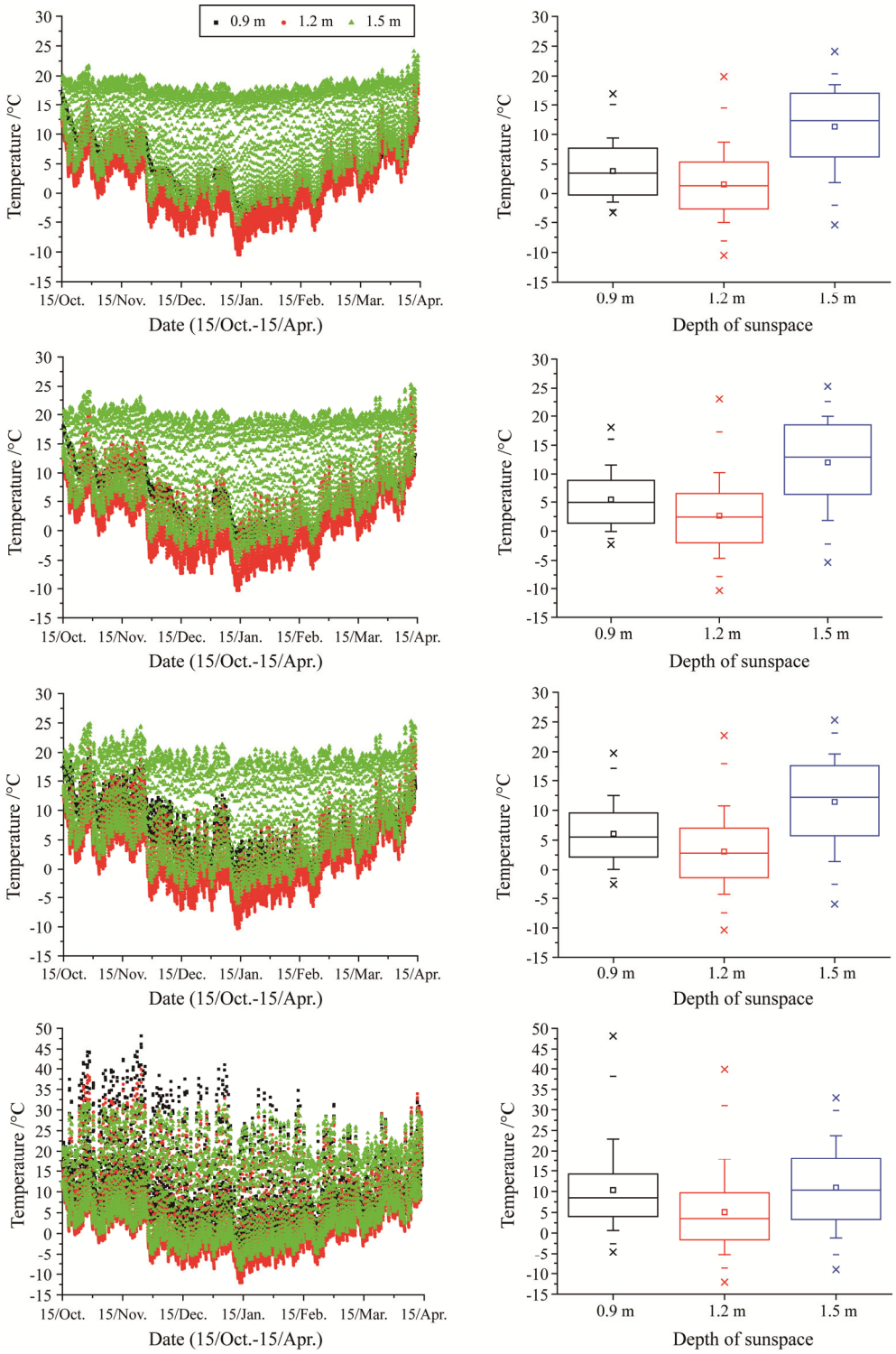

Fig. 7 The variations of hourly radiation temperatures with different depth of sunspace during heating season (*WWR* is 33%). (a) hourly temperature variation of room 1; (b) hourly temperature histogram of room 1; (c) hourly temperature variation of room 2; (d) hourly temperature histogram of room 2; (e) hourly temperature variation of room 3; (f) hourly temperature histogram of room 3; (g) hourly temperature variation of room 4; (h) hourly temperature histogram of room 4.

reached its highest value when the depth was 1.5 m, but underwent large-scale temperature fluctuations. The indoor temperature level corresponding to the sunspace depth of 0.9 m was lower, followed by that corresponding to the depth of 1.2 m. Temperature variations were significantly affected by cold months and the environment temperature, especially when the depths were 1.2 m and 1.5 m. Average temperature of Room 1 was around 4°C, 2°C and 11°C, when depths are 0.9 m, 1.2 m and 1.5 m, respectively. However, the average temperatures of Room 2 and Room 3 in buildings with different sunspace depths were about 5°C, 3°C and 12°C, slightly higher than that of Room 1, indicating that the influences of sunspace on Room 2 and Room 3 were greater than that on Room 1.

Room 4 could receive more solar heats to improve its indoor temperature, compared with other rooms. On the contrary, more heats would be lost through the transparent part of sunspace when the ambient temperature was lower. Besides, most heats were transferred through partitions between the sunspace and adjacent rooms (including Room 2, Room 3 and Room 5). During the day, specifically, the public door and window between the sunspace and Room 2 were opened, so that many heats were transferred into living room via air convection. Therefore, it can be revealed that the average radiation temperatures of Room 4, when sunspace depths were 0.9 m and 1.5 m, would be close (around 11°C). When the depth was 1.2 m, the average temperature (about 5°C) was the lowest, which was about 6°C lower than that of the previous two depths. The highest temperature (around 48°C) appeared when sunspace depth was 0.9 m, while the temperature fluctuation was larger, when the depths were 0.9 m and 1.2 m.

5. Discussion

Compared with other rooms, indoor radiation temperatures of Room 3, Room 4 and Room 5 were higher, since the sunspace and direct gain windows provided them with more possibilities to receive solar radiation (Figure 4). In comparison, less supported by solar radiation, northern rooms have lower radiation temperatures. Based on this, it is further proved that sunspace and direct gain windows played vital roles in improving indoor temperature and maintaining indoor thermal comfort.

Regarding the *WWRs* scenarios (Figure 6), temperatures reached their maximum values when *WWR* was 45%, followed by 33% and 60%, which indicated that 45% in *WWR* was the best setting to draw on indoor heat source and outdoor solar radiation for indoor thermal environment optimization. To be concrete, Room 3 and Room 5 in the case of *WWR*=60%, were directly exposed to solar radiation, due to the larger direct gain windows, resulting in higher temperatures, which however was offset by a sizeable proportion of heat dissipation at night when environmental temperature was low. Comparatively, both heat absorption and heat loss were less in the scenario of 33% in *WWR*, so that net heat was constrained at a low level. For the case of *WWR*=45%, direct gain windows in the daytime allowed sufficient solar heats to enter rooms, while they limited heat loss in the nighttime, comprehensively raising indoor temperatures. The results are in consistency with conclusions drawn in previous literature [46].

Goia et al. [47] found that the optimal *WWR* ranged between 35% and 45% in temperate oceanic climate zones regardless of building orientation. Thalfeldt et al. [48] discovered that 37.5% in *WWR* was responsible to the best energy performance. Nevertheless, a higher average temperature was obtained when *WWR* increased in Li's study [33]. The diurnal-nocturnal temperature differences of different regions might be an explanation for the result inconsistency.

The indoor temperature level was the highest when the depth was 1.5 m, compared with two other cases with different depths (Figure 7). This means much more solar radiation can access to the sunspace when the depth is 1.5 m, resulting in larger temperature differences between the sunspace and other rooms, than that in the cases of 0.9 m and 1.2 m in depth. The larger temperature difference is beneficial to drive more sunspace heats into other rooms, which can further enhance building heat storage. Whereas, it is supposed that heats transferred from rooms to outdoor environment via the sunspace were somewhat the same in all three scenarios in the nighttime because of the slow-paced process of heat dissipation. As a result, indoor thermal environment of rooms in the scenario of 1.5 m in depth was much higher. When the depths were 0.9 m and 1.2 m, in comparison, the solar radiation received was lower, further leading to lower temperature levels.

However, when it comes to the economic investment, a deeper sunspace that is surrounded by insulation materials requires higher initial investment, undermining its feasibility in actual projects. Therefore, some sunspaces adaptively adopt common materials, under which situation sunspace depth should be reduced to improve indoor thermal temperature level [32,49]. In contrast, the material used to construct sunspace in this study has excellent thermal insulation performance, so that its net heat was always positive. Understandably, more solar heats could be received and stored in the building with the increase of sunspace depth.

In addition, comparing models with sunspace depths of 0.9 m and 1.2 m (Figure 7), we found that the average radiation temperature of the former was slightly higher, while the temperature fluctuation of the latter was larger,

exhibiting that the heating preservation effect of the former was more outstanding. This depends on a combination result of heat absorption from outdoor environment and heat losses through the sunspace. Overall, the net heat of building with 0.9 m-depth sunspace was more than that with 1.2 m-depth sunspace, accounting for their average temperature differences.

This study investigates the effect of *WWR* and sunspace depth on the indoor thermal environment of passive solar houses in Qinghai-Tibetan region. Through critical analysis, the reasonable sunspace depth and *WWR* have been determined, which is valuable to inform HVAC engineers with understandings of optimizing dimensions of the direct gain window and the sunspace. Further, when building the passive house, the environment characteristics should be firstly surveyed, regarding the local solar radiation intensity, the variation of ambient temperature etc. Additionally, the materials of windows and sunspace have influence on the relationship between the thermal environment and *WWR* and depth as well. Therefore, the knowledge about design principles for passive solar house is also suitable for the other regions with similar climate, based on the materials with equivalent thermal insulation performances. However, what we have discussed in this study is not sufficient, for only the impacts of an individual factor on indoor temperature been analyzed. Consequently, indoor temperature under various conditions should be further explored, and the pattern of better dimensions of different building envelope remains to be studied.

6. Conclusions

This study comparatively examined the indoor radiation temperature, *PPD* and temperature characteristics of each room of a passive solar house in the Qinghai-Tibetan region. Based on the analysis in this study, several conclusions have been obtained.

(1) The reasonable design of sunspace and direct gain windows played a vital role in the improvement of indoor temperature and the maintenance of indoor thermal comfort level.

(2) The overall average radiation temperature of the building was approximately 16°C and *PPD* was in the range of 24%-44% for all rooms during the entire heating season, which could better satisfy the heating and thermal requirements under the condition of 0.9m/45%.

(3) The average radiation temperature of the passive solar house was higher, and its heating effect was better with the ratio of 45% (average radiation temperature approximately 17°C) or the depth of 1.5 m (average radiation temperature above 10°C) when the single factor of ratio or depth was considered.

However, how to match the ratio and depth to achieve a higher temperature level of the building requires further studies and analysis.

Acknowledgement

The research work was supported by National Key R&D Program of China-Technical System and Key Technology Development of Nearly Zero Energy Building (No. 2017YFC0702600), the opening Funds of State Key Laboratory of Building Safety and Built Environment National Engineering Research Center of Building Technology (BSBE2017-08), the Major Basic Research Development and Transformation Program of Qinghai province (No. 2016-NN-141) and the Fundamental Research Funds for the Central Universities (No. 2018MS103, 2018MS108 and 2017MS119).

References

[1] Zhao D., Ji J., Yu H., Wei W., Zheng H. Numerical and experimental study of a combined solar Chinese kang and solar air heating system based on Qinghai demonstration building. Energy and Buildings, 2017, 143: 61–70.

[2] Yang L., He B., Ye M. The application of solar technologies in building energy efficiency: BISE design in solar-powered residential buildings. Technology in Society, 2014, 38: 111–118.

[3] Zhao D.X., He B.J., Johnson C., Mou B. Social problems of green buildings: From the humanistic needs to social acceptance. Renewable & Sustainable Energy Reviews, 2015, 51: 1594–1609.

[4] Nejat P., Jomehzadeh F., Taheri M.M., Gohari M., Muhd M.Z. A global review of energy consumption, CO_2 emissions and policy in the residential sector (with an overview of the top ten CO_2 emitting countries). Renewable & Sustainable Energy Reviews, 2015, 43: 843–862.

[5] Marino, C., Nucara, A., Pietrafesa, M. Does window-to-wall ratio have a significant effect on the energy consumption of buildings? A parametric analysis in Italian climate conditions. Journal of Building Engineering, 2017, 13: 169– 183.

[6] Baglivo C., Congedo P.M., Di Cataldo M., Coluccia L.D., D'Agostino D. Envelope design optimization by thermal modelling of a building in a warm climate. Energies, 2017, 10(11): 1808.

[7] Mou B., He B.J., Zhao D.X., Chau K. Numerical simulation of the effects of building dimensional variation on wind pressure distribution. Engineering Applications of Computional Fluid Mechanics, 2017, 11: 293–309.

[8] Liu Z., Cheng K., Li H., Cao G., Wu D., Shi Y. Exploring the potential relationship between indoor air quality and

the concentration of airborne culturable fungi: a combined experimental and neural network modeling study. Environmental Science and Pollution Research, 2018, 25(4): 3510-3517.

[9] Hua W., Fan G.Z., Zhou D.W., Chen Q.L. Analysis on the variation trend of interannual and interdecadal seasonal sunshine duration over Tibetan plateau. Journal of Natural Resources, 2009, 24: 1810–1817.

[10] Rodriguez-Ubinas E., Montero C., Porteros M., Vega S., Navarro I., Castillo-Cagigal M., Matallanas E., Gutierrez A. Passive design strategies and performance of Net Energy Plus Houses. Energy and Buildings, 2014, 83: 10–22.

[11] Tong G., Christopher D.M., Li T., Wang T. Passive solar energy utilization: A review of cross-section building parameter selection for Chinese solar greenhouses. Renewable & Sustainable Energy Reviews, 2013, 26: 540–548.

[12] Li H., Liu Z., Liu K., Zhang Z. Predictive Power of Machine Learning for Optimizing Solar Water Heater Performance: The Potential Application of High-Throughput Screening. International Journal of Photoenergy, 2017, (2017): 1–10.

[13] Liu Z., Xu W., Zhai X., Qian C., Chen X. Feasibility and performance study of the hybrid ground-source heat pump system for one office building in Chinese heating dominated areas. Renewable Energy, 2017, 101: 1131–1140.

[14] Li D.S., Tan M.L., Zhang S.F., Ou J.P. Stress corrosion damage evolution analysis and mechanism identification for prestressed steel strands using acoustic emission technique. Structural Control Health Monitoring, 2018, e2189.

[15] Liu Z., Wu D., Yu H., Ma W., Jin G. Field measurement and numerical simulation of combined solar heating operation modes for domestic buildings based on the Qinghai–Tibetan plateau case. Energy and Buildings, 2018, 167: 312–321.

[16] Zhao Z.Q., He B.J., Li L.G., Wang H.B., Darko A. Profile and concentric zonal analysis of relationships between land use/land cover and land surface temperature: Case study of Shenyang, China. Energy and Buildings, 2017, 155: 282-295.

[17] Gao R., Fang Z., Li A., Liu K., Yang Z., Cong B. A novel low-resistance tee of ventilation and air conditioning duct based on energy dissipation control. Applied Thermal Engineering, 2018, 132: 790–800.

[18] Salvalai G., Zambelli E. A case study of low-energy houses in Northern Italy. In CESB 2010 Prague - Central Europe towards Sustainable Building “From Theory to Practice”, 2010, pp. 1–9.

[19] Liu J. Experimental study on passive solar house in Qinghai-Tibet plateau region. Solar Energy, 2011, 19: 45–48.

[20] Rekstad J., Meir M., Murtnes E., Dursun A. A comparison of the energy consumption in two passive houses, one with a solar heating system and one with an air-water heat pump. Energy and Buildings, 2015, 96: 149–161.

[21] Shan M., Yu T., Yang X. Assessment of an integrated active solar and air-source heat pump water heating system operated within a passive house in a cold climate zone. Renewable Energy, 2016, 87: 1059–1066.

[22] He W., Hong X., Wu X., Pei G., Hu Z., Tang W., Shen Z., Ji J. Thermal and hydraulic analysis on a novel Trombe wall with venetian blind structure. Energy and Buildings, 2016, 123: 50–58.

[23] Bellos E., Tzivanidis C., Zisopoulou E., Mitsopoulos G., Antonopoulos K.A. An innovative Trombe wall as a passive heating system for a building in Athens—A comparison with the conventional Trombe wall and the insulated wall. Building and Environment, 2016, 133: 754–769.

[24] Gao R., Liu K., Li A., Fang Z., Yang Z., Cong B. Biomimetic duct tee for reducing the local resistance of a ventilation and air-conditioning system. Building and Environment, 2018, 129: 130–141.

[25] Liu Z., Li H., Liu K., Yu H., Cheng K. Design of high-performance water-in-glass evacuated tube solar water heaters by a high-throughput screening based on machine learning: A combined modeling and experimental study. Solar Energy, 2017, 142: 61–67.

[26] Lee J.W., Jung H.J., Park J.Y., Lee J.B., Yoon Y. Optimization of building window system in Asian regions by analyzing solar heat gain and daylighting elements. Renewable Energy, 2013, 50: 522–531.

[27] Yu J., Yang C., Tian L. Low-energy envelope design of residential building in hot summer and cold winter zone in China. Energy and Buildings, 2008, 40: 1536–1546.

[28] Lu C., Tang R. Analyzing energy efficiency of solar-house attached sunsapces in the cold region. Energy Conservation, 2005, 7: 28–30.

[29] Zhang X.F., Niu S.W., Luo G.H., Yang L.N. The heating effect of the additional solar house to classroom in the cold region—A case study of an elementary school. Energy Procedia, 2012, 14: 1193–1198.

[30] Chiesa G., Simonetti M., Ballada G. Potential of attached sunspaces in winter season comparing different technological choices in Central and Southern Europe. Energy and Buildings, 2017, 138: 377–395.

[31] Bataineh K.M., Fayez N. Analysis of thermal performance of building attached sunspace. Energy and Buildings, 2011, 43: 1863–1868.

[32] Schoenau G.J., Lumbis A.J., Besant R.W. Thermal performance of four sunspaces in a cold climate. Energy and Buildings, 1990, 14: 273–286.

[33] Li E., Liu J.P., Yang L. Research on the Passive Design Optimization of Direct Solar Gain House for Residential Buildings in Lhasa. Industrial Construction, 2012, 42: 27–32.

[34] Yu H., Dang J., Ma W. Technical Specification for Passive Solar Heating in Qinghai Province (DB63/T 1527-2016), Qinghai, China, 2017.

[35] Liu Z., Wu D., Jiang M., Yu H., Ma W. Field measurement and evaluation of the passive and active solar heating systems for residential building based on the Qinghai-Tibetan Plateau Case. Energies, 2017, 10(11): 1706.

[36] Aldossary N.A., Rezgui Y., Kwan A. Domestic energy consumption patterns in a hot and arid climate: A multiple-case study analysis. Renewable Energy, 2014, 62: 369–378.

[37] Azhar S., Brown J. Bim for sustainability analyses. International Journal of Construction Education and Research, 2009, 5: 276–292.

[38] Kim G., Lim H.S., Lim T.S., Schaefer L., Kim J.T. Comparative advantage of an exterior shading device in thermal performance for residential buildings. Energy and Buildings, 2012, 46: 105–111.

[39] Lau A.K.K., Salleh E., Lim C.H., Sulaiman M.Y. Potential of shading devices and glazing configurations on cooling energy savings for high-rise office buildings in hot-humid climates: The case of Malaysia. International Journal of Sustainable Built Environment, 2016, 5: 387–399.

[40] Bi Y., Chen L., Ding Z. Performance optimization of irreversible air heat pumps considering size effect. Journal of Thermal Science, 2018, 27(3): 223-229.

[41] Xiao W. Study of the direct-gain solar heating in remote southwest Tibet, Tsinghua University, Beijing, China, 2010.

[42] Zhu Y.X. Building Environment, 3rd ed., Architecture & Building Press: Beijing, China, 2005.

[43] Park K.S., Kim S.W., Yoon S.H. Application of breathing architectural members to the natural ventilation of a passive solar house. Energies 2016, 9: 214.

[44] Hugo A., Zmeureanu R. Residential solar-based seasonal thermal storage systems in cold climates: building envelope and thermal storage. Energies, 2012, 5: 3972–3985.

[45] Osborne A., Baur S., Grantham K. Simulation prototyping of an experimental solar house. Energies 2010, 3: 1251–1262.

[46] Li G., Xuan Q., Pei G., Su Y., Ji J. Effect of non-uniform illumination and temperature distribution on concentrating solar cell - A review. Energy, 2018, 144: 1119–1136.

[47] Goia F., Haase M., Perino M. Optimizing the configuration of a façade module for office buildings by means of integrated thermal and lighting simulations in a total energy perspective. Applied Energy, 2013, 108: 515– 527.

[48] Thalfeldt M., Pikas E., Kurnitski J., Voll H. Facade design principles for nearly zero energy buildings in a cold climate. Energy and Buildings, 2013, 67: 309–321.

[49] Monge-Barrio A., Sánchez-Ostiz A. Energy efficiency and thermal behaviour of attached sunspaces, in the residential architecture in Spain. Summer Conditions. Energy and Buildings, 2015, 108: 244–256.